Chinese Chemical Letters 34 (2023) 108052

Contents lists available at ScienceDirect

Chinese Chemical Letters

journal homepage: www.elsevier.com/locate/cclet

Ultrathin two-dimensional porphyrinic metal-organic framework nanosheets induced by the axial aryl substituent

Jurong Dong, Yufei Wang, Yu-Lin Lu, Li Zhang*

MOE Laboratory of Bioinorganic and Synthetic Chemistry, Lehn Institute of Functional Materials, School of Chemistry, Sun Yat-Sen University, Guangzhou 510006, China

ARTICLE INFO

Article history:
Received 19 August 2022
Revised 6 December 2022
Accepted 6 December 2022
Available online 8 December 2022

Keywords:
Metalloporphyrin
Axial aryl substituent
2D MOF nanosheets
CO_2 transformation
Heterogeneous catalysis

ABSTRACT

Ultrathin two-dimensional metal-organic framework nanosheets have emerged as a promising kind of heterogeneous catalysts. Herein, we report a new kind of 2D porphyrinic metal-organic framework nanosheets of Rh2-PCN-222, which was prepared from the self-assembly of the metalloporphyrin ligand Rh(TCPP)(DCB) (TCPP = 5,10,15,20-tetrakis(4-methoxycarbonylphenyl)porphyrin; DCB = 3,4-dichlorobenzene) and $ZrCl_4$ in the presence of two kinds of monocarboxylic acids as the modulating reagent. The thickness of Rh2-PCN-222 nanosheets was characterized by atomic force microscopy (AFM) and determined to be 5.4-9.6 nm. It was found that the axial aryl dichlorophenyl substituent, which controlled the anisotropic growth of MOFs, was essential for the formation of nanosheets. Catalytic results showed that Rh2-PCN-222 nanosheets were efficient for CO_2 transformation.

As a new class of materials with ultrathin thickness, large surface area, highly accessible active sites and rich options for metal ions and organic ligands, two-dimensional (2D) metal-organic framework (MOF) nanosheets have fascinated researchers in their synthesis strategies and applications in separation, catalysis, sensing, electronic devices, *etc.* [1–5]. Particularly in the field of heterogeneous catalysis, 2D MOF nanosheets display high catalytic performances due to the exposed active sites on the external surfaces, which can well interact with the substrates and then efficiently promote the catalytic reactions without diffusion constraints [6–9]. Nevertheless, the synthesis of 2D MOFs still remains a great challenge, requiring the selective growth of MOF crystals in the lateral directions rather than along the vertical direction [10–18].

Being one of the most frequently found species in nature, porphyrins have been used as linkers, giving rise to porphyrinic metal-organic frameworks (PMOFs) [19–23]. Porphyrins can accommodate various elements in the periodic table, ranging from transition metals to main group elements, and therefore, the catalytic functionalities of PMOFs can be easily realized by modulating the central atoms within the porphyrin macrocycles [24–26]. Up to now, many 3D crystalline PMOFs with different topological structures have been studied [27–41]. However, due to the rigid and robust features of porphyrin-based ligands, it is of high challenge for their anisotropic growth to generate 2D PMOFs, and especially the non-layer structured 2D PMOF nanosheets, which are reported to be synthesized by a series of bottom-up methods, including interfacial synthesis [42,43], layer-by-layer growth [44–46], surfactant-assisted synthesis [47–54] and modulated synthesis [55–58]. Recently, our group has developed a new ligand mismatch method, in which the formation of 2D MOF sheets is controlled by the ligand's mismatch, giving rise to anisotropic growth [59].

Herein, we report the preparation of a new 2D Rh-porphyrin metal-organic framework nanosheet, which is denoted as Rh2-PCN-222, through the self-assembly of the metalloporphyrin ligand Rh(TCPP)(DCB) (TCPP = 5,10,15,20-tetrakis(4-methoxycarbonylphenyl)porphyrin; DCB = 3,4-dichlorobenzene) and $ZrCl_4$ in the presence of two kinds of monocarboxylic acids as the modulating reagent. The selection of the porphyrin ligand Rh(TMCPP)(DCB) with axial dichlorophenyl substituent is crucial for the synthesis of 2D porphyrinic MOF nanosheets of Rh2-PCN-222 with csq topology. The axial substituent restricts the growth of MOFs in one of three dimensions due to the large steric hindrance. The 2D Rh2-PCN-222 nanosheets display excellent thermal and chemical stability, and the framework and crystallinity of Rh2-PCN-222 nanosheets remain well upon combination with metal nanoparticles by the *in situ* formation. Catalytic results showed that it behaved as an efficient heterogeneous catalyst for the chemical fixation of CO_2 into cyclic carbonates under mild conditions (Fig. 1).

5,10,15,20-Tetrakis(4-methoxycarbonyl phenyl)porphyrin rhodium (III) 3,4-dichlorobenzene (Rh(TMCPP)(DCB)) was synthesi-

* Corresponding author.
E-mail address: zhli99@mail.sysu.edu.cn (L. Zhang).

https://doi.org/10.1016/j.cclet.2022.108052
1001-8417/

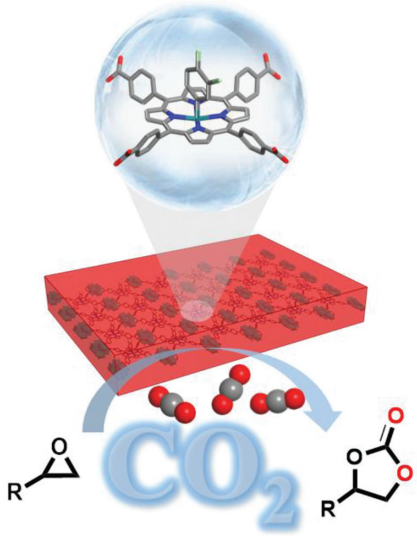

Fig. 1. Schematic illustration of the structure and catalytic behavior of Rh2-PCN-222.

zed by the reaction of 5,10,15,20-tetrakis(4-methoxycarbonylphenyl)porphyrin (TMCPP) and $[Rh(COD)Cl]_2$ in the molar ratio of 1:1.3 and in 1,2,4-trichlorobenzene at 196-200 °C for 72 h (Fig. 2a and Scheme S1 in Supporting information). It is noted that in addition to the major product of Rh(TMCPP)(DCB) (~39% yield), the minor product of Rh(TMCPP)Cl (~7% yield) was also generated. The structure of Rh(TMCPP)(DCB) with an unsaturated five-coordination mode of the Rh center has been confirmed by the X-ray single crystallography (CCDC: 2168326) (Fig. 2b). The crystal structure refinement data and selected bond angles and distances are listed in Tables S1 and S2 (Supporting information), respectively. Afterwards, the hydrolysis of Rh(TMCPP)(DCB) in KOH solution afforded 5,10,15,20-tetrakis(4-carboxyphenyl)porphyrin rhodium(III) 3,4-dichlorobenzene (Rh(TCPP)(DCB)).

A plausible formation mechanism was proposed (Fig. 2c). Firstly, $[Rh(COD)Cl]_2$ reacted with TMCPP to yield Rh(TMCPP)Cl, which then reacted with water contaminated in the solvent of 1,2,4-trichlorobenzene at 196-200 °C to generate Rh(TMCPP)OH [60–64]. During the proposed process, HCl should be generated, whose formation was confirmed *via* examination of the pH (~2) of the evolved gas from the reaction flask (Figs. S1 and S2 in Supporting information). Rh(TMCPP)OH then rapidly converted to $[Rh(TMCPP)]_2$ and H_2O_2. Considering that the bond dissociation energy of Ar-Cl bond (95 kcal/mol) [65] is lower than the Ar-H bond (113 kcal/mol) [66], $[Rh(TMCPP)]_2$ preferred to cleave the C-Cl bond of 1,2,4-trichlorobenzene to give Rh(TMCPP)(DCB) and Rh(TMCPP)Cl [67–69].

The X-ray photoelectron spectroscopy (XPS) analyses showed that the valence of the central Rh atom in Rh(TCPP)(DCB) was in the range of +2~+3, whose binding energies were located at 309.44 and 309.70 eV for Rh $3d_{5/2}$ and 314.04 and 314.65 eV for Rh $3d_{3/2}$ (Fig. S3a in Supporting information). It was different from the typical +3 charge in Rh(TCPP)Cl, which might be due to the lower electronegativity of C (2.55) than Cl (3.16) and thus endowed the Rh-C bond with covalent character. The XPS analyses further disclosed that there were no Rh-Cl bonds in Rh(TCPP)(DCB), because Cl $2p_{1/2}$ and Cl $2p_{3/2}$ in Rh(TCPP)(DCB) were shifted to a higher binding energy by about 2.6 eV compared to Rh(TCPP)Cl (Figs. S3b-d in Supporting information), which was consistent with the literature reports [70–73].

The existence of the axial dichlorophenyl substituent was further confirmed by the ATR-IR spectra (Fig. S4 in Supporting information). Compared to Rh(TCPP)Cl, a new absorption peak around 1455 cm^{-1} appeared in the ATR-IR spectrum of Rh(TCPP)(DCB), which was assigned to the C-H bending vibration of 1,2,4-trichlorobenzene [74].

UV-vis absorption spectra were further examined (Fig. S5 and Table S3 in Supporting information). Rh(TCPP)(DCB) displayed significant Q-band absorption at 526.5 nm and a weak absorption peak at 561.5 nm. The Soret and Q bands of Rh(TCPP)(DCB) appeared blue-shifted compared to Rh(TCPP)Cl, that is from 419 nm

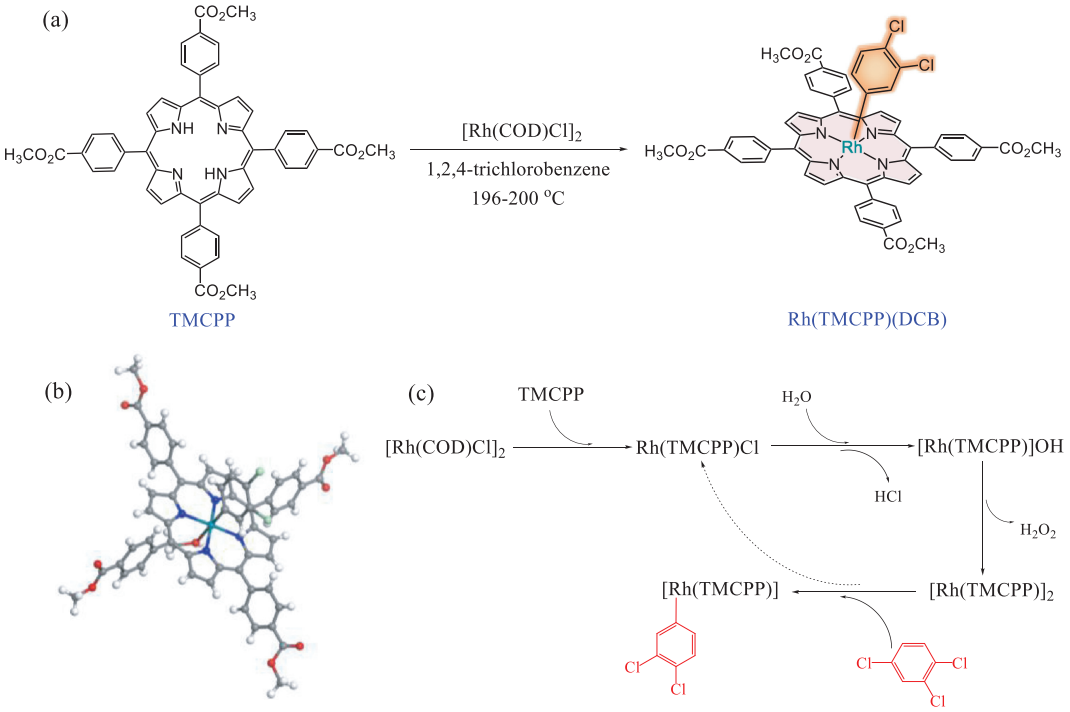

Fig 2. The synthesis (a), crystal structure (b) and possible formation mechanism (c) of Rh(TMCPP)(DCB).

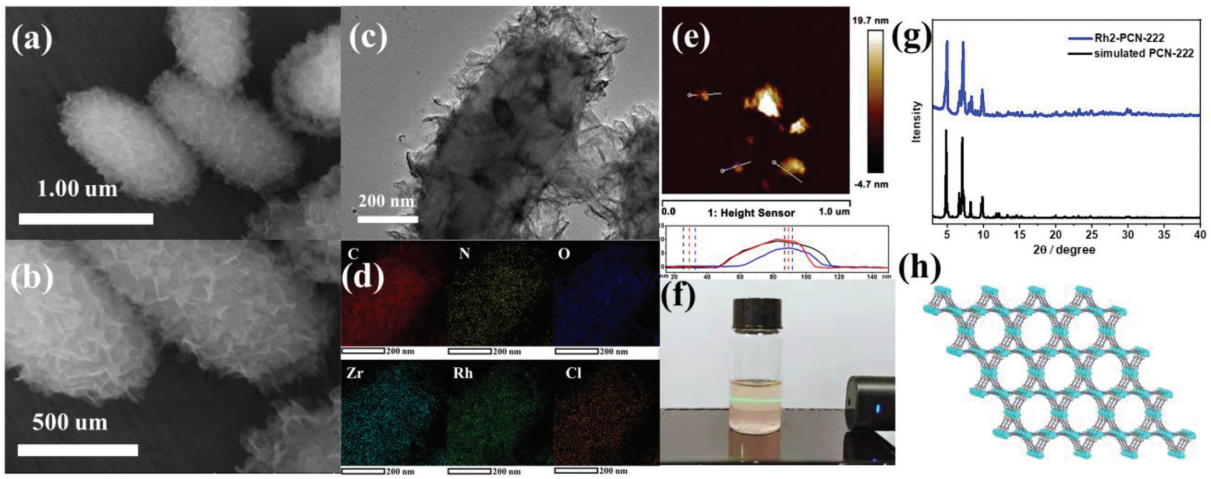

Fig. 3. SEM (a, b), TEM (c), TEM-EDX elemental mapping (d), AFM (e), the Tyndall effect image (f), PXRD patterns (g) and the simulated crystal structure (h) of Rh2-PCN-222.

to 414 nm and from 531 nm to 527 nm, respectively. The UV-vis absorption spectra of Rh(TCPP)(DCB) film and Rh(TCPP)Cl film were also examined (Fig. S5c and Table S4 in Supporting information). The metalloporphyrin film was prepared by a simple solution-processing *quasi*-Langmuir-Shäfer (QLS) method [75]. It could be found that the Soret and Q bands of Rh(TCPP)(DCB) film also displayed blue shift compared to Rh(TCPP)Cl film. This indicated that Rh(TCPP)(DCB) was more inclined to H aggregation and face-to-face π-π interaction among tetrapyrrole rings (Fig. S6 in Supporting information) [76,77].

The self-assembly of Rh(TCPP)(DCB) and $ZrCl_4$ in the presence of acetic acid and benzoic acid at 120 °C for 24 h gave rise to 2D Rh2-PCN-222 nanosheets. The morphology and structure of Rh2-PCN-222 were investigated by various characterization techniques. The scanning electron microscope (SEM) and transmission electron microscopy (TEM) images disclosed that the inner core of Rh2-PCN-222 was of the rod-like morphology whereas the outer was covered with nanosheets (Figs. 3a-c). It was noted that when the reaction mixture was heated for 6 h, uniform nanosheets were formed (Figs. S7a-c in Supporting information). Prolonging the reaction time to 12 h and then 24 h, the inner nanosheets gradually aggregated into rods but the outer nanosheets remained (Figs. S7d-f in Supporting information).

Energy dispersive X-ray spectroscopy (EDS) revealed that Cl, Rh and Zr elements existed in Rh2-PCN-222 and the atomic ratio of Cl:Rh was around 2:1 (Fig. 3d, Figs. S8 and S9 and Table S5 in Supporting information). The thickness of Rh2-PCN-222 nanosheets was characterized by atomic force microscopy (AFM) and determined to be 5.4-9.6 nm (Fig. 3e). The suspension of Rh2-PCN-222 in ethanol showed the typical Tyndall effect when a green laser passes through it, indicative of the colloidal structures (Fig. 3f).

Then, the structure of Rh2-PCN-222 was confirmed by the powder X-ray different (PXRD) patterns, which fit well with the simulated patterns from the reported crystal structures of PCN-222 (Figs. 3g and h) [78]. The weak diffraction intensity of peak was ascribed to the nature of two-dimension nanosheets, which was similar to other 2D-MOF materials. The surface area and porosity of Rh2-PCN-222 were evaluated using N_2 adsorption-desorption isotherms at 77 K (Fig. S10 in Supporting information). The type I isotherms indicated the microporosity of the structure. The Brunauer-Emmett-Teller (BET) surface areas of Rh2-PCN-222 were calculated to be 1342 m^2/g. The XPS spectra of Rh2-PCN-222 showed that the valence of Rh atoms was in the range of +2∼+3, and the ratio of Rh^{2+} and Rh^{3+} was calculated to be 65:35 (Fig. S11 in Supporting information). In addition, there was no Rh-Cl bond.

Rh2-PCN-222 exhibited good thermal stability and could be stable up to 347 °C as suggested by the thermal gravimetric (TG) analysis (Fig. S12 in Supporting information). The thermal stability of Rh2-PCN-222 was further explored by the variable temperature VT-PXRD measurement, which suggested that the crystallinity of its framework could be maintained up to 300 °C (Fig. S13 in Supporting information). In addition, Rh2-PCN-222 possessed good chemical stability. After the samples were soaked in organic solvents such as acetone, dichloromethane (DCM), methanol, acetonitrile (MeCN) and ethyl acetate for one week, the PXRD patterns remained (Fig. S14 in Supporting information). Upon digestion, the ^1H NMR spectroscopy of the dissolved Rh2-PCN-222 was consistent with the ligand Rh(TCPP)(DCB) before MOF synthesis, suggesting that Rh(TCPP)(DCB) was stable during the MOF synthesis (Fig. S15 in Supporting information).

The formation mechanism of Rh2-PCN-222 nanosheets was studied, which was mainly influenced by two aspects. On one hand, the design of Rh(TCPP)(DCB) was inspired by the surfactant-assisted synthetic method (Fig. 4). The axial dichlorophenyl substituent displayed similar effects to surfactants such as PVP, which could selectively cap the top faces of the MOFs, prevent the crystals from growing along the axial direction due to the steric hindrance and then lead to the formation of ultrathin MOF nanosheets. For comparison, the self-assembly of Rh(TCPP)Cl and $ZrCl_4$ could only give rise to rod-shaped crystals (that is named after Rh1-PCN-222) instead of nanosheets (Fig. S16 in Supporting information).

On the other hand, modulators are also widely used in the synthesis of MOFs. During the synthesis, the metal nodes first react with modulators at the nucleation stage and then MOF crystals form by the exchange of the modulators with the organic ligands. In this work, Rh2-PCN-222 nanosheets could not be obtained by using a single monocarboxylic acid (*e.g.,* formic acid, acetic acid and trifluoroacetic acid) as the modulator (Fig. S17 in Supporting information). When benzoic acid was used as the sole modulator, no crystal could be formed at all. To our delight, the desired Rh2-PCN-222 nanosheets were obtained using acetic acid and benzoic acid as the double modulator (Figs. 3a-c). However, when other couples of monocarboxylic acids such as benzoic acid/formic acid and benzoic acid/trifluoroacetic acid were employed as the modulators, 3D rod-shaped MOF were produced instead (Fig. S18 in Supporting information).

The MOF composites Ag/Rh2-PCN-222, Au/Rh2-PCN-222 and Pd/Rh2-PCN-222 were prepared by the *in situ* formation of metal nanoparticles (M NPs) at the surface of Rh2-PCN-222, which

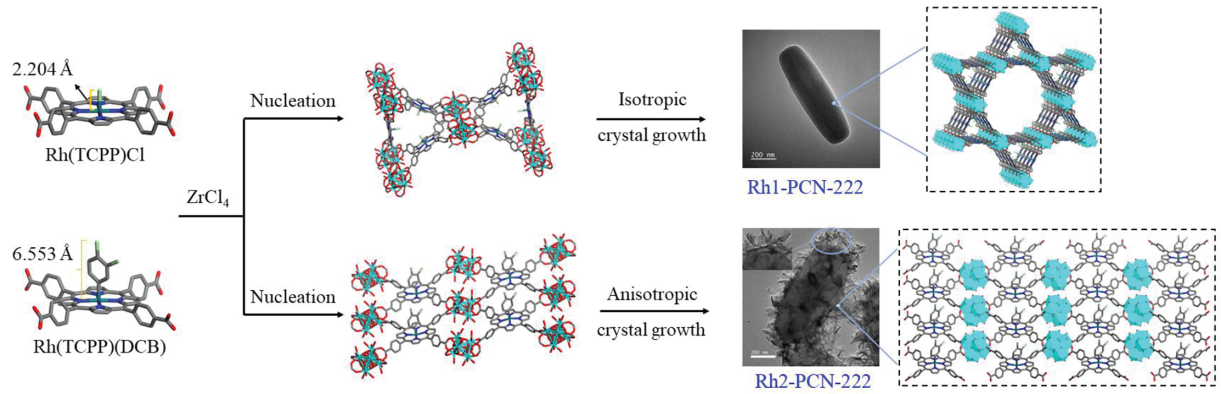

Fig. 4. The syntheses and structures of Rh1-PCN-222 and Rh2-PCN-222.

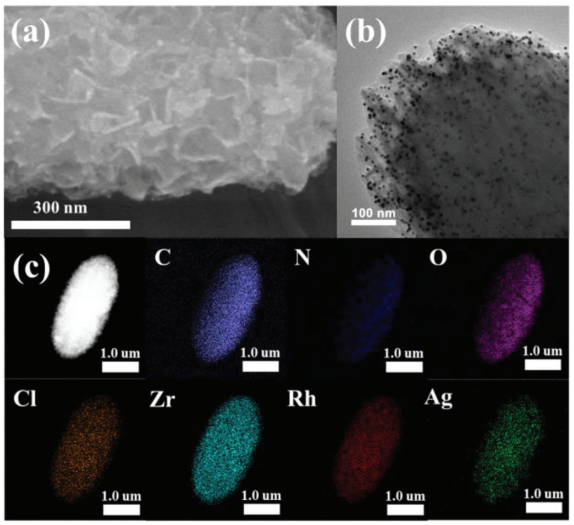

Fig. 5. SEM (a), TEM (b), TEM-EDX elemental mapping (c), image of the as-synthesized Ag/Rh2-PCN-222.

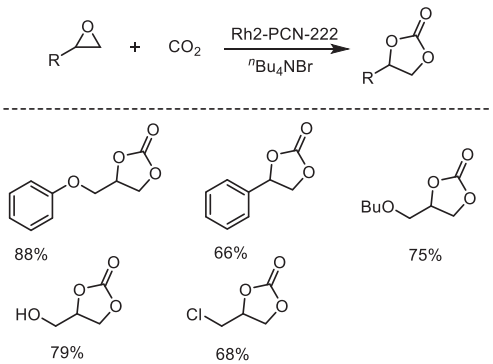

Scheme 1. Cycloaddition reactions of different substituted epoxides and CO_2 promoted by Rh2-PCN-222. Reaction conditions: epoxide (1 mmol), catalyst (0.0058 mmol), $^{n}Bu_4NBr$ (0.002 mmol), at 100 °C, under 1 bar CO_2, 24 h. The yield is determined by ^1H NMR of the crude residue.

were accomplished by the solvothermal reaction of Rh2-PCN-222 and metal salts of $AgNO_3$, $HAuCl_4$ and Na_2PdCl_4, respectively, with polyvinyl pyrrolidone (PVP) in DMF at 125 °C for 30 min. SEM and TEM images showed that metal nanoparticles were uniformly dispersed on the surface of Rh2-PCN-222 (Figs. 5a and b, Fig. S19 in Supporting information). Meanwhile, the TEM-EDX elemental mapping images demonstrated the presence and uniform distribution of all of the elements in the composites of M NPs/Rh2-PCN-222 (Fig. 5c and Fig. S20 in Supporting information). The PXRD patterns of M NPs/Rh2-PCN-222 matched with those of Rh2-PCN-222, indicating that the framework and crystallinity of Rh2-PCN-222 remained upon the combination with metal nanoparticles (Fig. S21 in Supporting information). The metallic species with zero charge were clearly identified. As shown in the XPS spectra of Ag/Rh2-PCN-222, the binding energies at 368.15 and 374.15 eV were assignable to the $3d_{5/2}$ and $3d_{3/2}$ levels of Ag(0), respectively (Fig. S22 in Supporting information). It is noted that the Ag NPs on Rh2-PCN-222 were more stable than on Rh1-PCN-222, indicating that the folded nanosheets provided better support to load metal nanoparticles (Fig. S23 in Supporting information).

Rh2-PCN-222 displayed good CO_2 adsorption capability, and the amounts of CO_2 were 23.8 and 42.1 cm^3/g at 1 bar at 273 and 298 K, respectively (Fig. S24a in Supporting information) [79]. The corresponding isosteric adsorption enthalpy (Q_{st}) value was 24.86 kJ/mol at zero coverage by the virial fitting method (Fig. S24b in Supporting information) [80], which was competent to the reported porphyrinic MOFs such as 2D MOF-NS-Co (22.1 kJ/mol) [58], PCN-601 (21.7 kJ/mol) [81], indicating that Rh2-PCN-222 exhibited strong affinity towards CO_2 and the higher CO_2-philicity would be crucial for the catalytic conversion of CO_2. It was noted that the Q_{st} values of CO_2 remained approximately constant as the CO_2 loading increased, indicating that adsorption sites for CO_2 on Rh2-PCN-222 were of uniform distribution [82].

The good CO_2 adsorption uptakes of Rh2-PCN-222 promoted us to investigate its catalytic performance of the cycloaddition of CO_2 with epoxides for the efficient formation of cyclic carbonates under mild conditions. The reaction of 2-(phenoxymethyl)oxirane and CO_2 was chosen as the model reaction. Rh2-PCN-222 was an efficient catalyst for the cycloaddition reaction with up to 88% conversion of epoxide to 4-phenoxymethyl-1,3-dioxolan-2-one under 1 bar and 100 °C for 24 h. The high catalytic performances could be kept when using different batches of as-synthesized Rh2-PCN-222 (Table S6 in Supporting information). For comparison, PCN-222 built with metal-free porphyrin ligand displayed 37% yield under similar reaction conditions. In the absence of any catalyst, the conversion decreased significantly to only 29%. Therefore, the rhodium-porphyrin was the catalytic site.

The catalytic reactions of CO_2 and epoxides containing other functional groups were also carried out, including 2-phenyloxirane, 2-(butoxymethyl)oxirane, oxiran-2-ylmethanol and 2-(chloromethyl)oxirane. These catalytic reactions proceeded smoothly and gave rise the corresponding cyclic carbonates with yields of 66%-88% with larger than 99% selectivity (Scheme 1).

The high thermal and chemical stability of Rh2-PCN-222 helped it to behave as a robust and truly heterogeneous catalyst. After the catalytic reaction, the crystalline catalyst samples were isolated from the reaction mixture by centrifugation and reused for 3 times without significant loss of activity (Fig. S25 in Supporting information). Before each run, the Rh2-PCN-222 catalyst was washed with dichloromethane to remove the absorbed organic compounds on the exterior surfaces. During the three reaction runs, the yield of the cyclic carbonate product remained around 88%. The PXRD patterns of the recycled Rh2-PCN-222 nanosheets were retained after catalysis (Fig. S26 in Supporting information). Analysis of the filtrate after catalytic reactions by inductively coupled plasma-atomic emission spectrometry (ICP-AES) indicated that the amounts of Rh and Zr leaching into the reaction solution were 0.23% and 0.86%, respectively. In addition, after catalytic reaction, Rh2-PCN-222 was recycled and dissolved in $(CD_3)_2SO$. The ^1H NMR spectrum showed that the axial aryl substituent (DCB) was present in the recycled Rh2-PCN-222 sample after catalysis (Fig. S27 in Supporting information).

In summary, through C-Cl bond dissociation, a new metalloporphyrin ligand Rh(TCPP)(DCB) with the dichlorophenyl substituent in the axial position was prepared. Self-assembly of Rh(TCPP)(DCB) and $ZrCl_4$ in the presence of a double modulating agent led to the formation of 2D Rh2-PCN-222 nanosheets. This newly developed synthesis protocol of 2D MOFs can avoid the uses of the surfactant molecules, which might block the active sites. The prepared 2D Rh2-PCN-222 nanosheets displayed good CO_2 adsorption capability and behaved as an efficient heterogeneous catalyst towards CO_2 transformations. Further work about the design and catalytic applications of the 2D porphyrinic MOFs are in process.

Declaration of competing interest

The authors declare that they have no known competing financial interests or personal relationships that could have appeared to influence the work reported in this paper.

Acknowledgments

The authors acknowledge support from the National Natural Science Foundation of China (Nos. 21773314, 21821003 and 21890382), the Guangdong Natural Science Funds for Distinguished Young Scholar (No. 2019B151502017).

Supplementary materials

Supplementary material associated with this article can be found, in the online version, at doi:10.1016/j.cclet.2022.108052.

References

[1] M. Zhao, Q. Lu, Q. Ma, H. Zhang, Small Methods 1 (2017) 1600030.
[2] Y.Z. Li, Z.H. Fu, G. Xu, Coord. Chem. Rev. 388 (2019) 79–106.
[3] W. Zhao, J. Peng, W. Wang, et al., Coord. Chem. Rev. 377 (2018) 44–63.
[4] Q. Jiang, C. Zhou, H. Meng, et al., J. Mater. Chem. A 8 (2020) 15271–15301.
[5] Y. Zheng, F.Z. Sun, X. Han, J. Xu. X.H. Bu, Adv. Optical Mater. 8 (2020) 2000110.
[6] A. Dhakshinamoorthy, A.M. Asiri, H. Garcia, Adv. Mater. 31 (2019) 1900617.
[7] C. Tan, G. Liu, H. Li, Y. Cui, Y. Liu, Dalton Trans. 49 (2020) 11073–11084.
[8] J. Nicks, K. Sasitharan, R.R.R. Prasad, D.J. Ashworth, J.A. Foster, Adv. Funct. Mater. 31 (2021) 2103723.
[9] G. Chakraborty, I.H. Park, R. Medishetty, J.J. Vittal, Chem. Rev. 121 (2021) 3751–3891.
[10] Y. Peng, Y. Li, Y. Ban, et al., Science 346 (2014) 1356–1359.
[11] G. Zhan, H.C. Zeng, Adv. Funct. Mater. 26 (2016) 3268–3281.
[12] L. Cao, Z. Lin, F. Peng, et al., Angew. Chem. 128 (2016) 5046–5050.
[13] D. Zhu, C. Guo, J. Liu, et al., Chem. Commun. 53 (2017) 10906–10909.
[14] M. Yuan, R. Wang, W. Fu, et al., ACS Appl. Mater. Interfaces 11 (2019) 11403–11413.
[15] X. Zhang, P. Zhang, C. Chen, et al., Green Chem. 21 (2019) 54–58.
[16] S. Jiang, X. Shi, Y. Zu, F. Sun, G. Zhu, Mater. Chem. Front. 5 (2021) 5150–5157.
[17] M. Hu, J. Liu, S. Song, et al., ACS Catal. 12 (2022) 3238–3248.
[18] Q. Deng, X. Hou, Y. Zhong, et al., Angew. Chem. Int. Ed. 61 (2022) e202205453.
[19] W.Y. Gao, M. Chrzanowski, S. Ma, Chem. Soc. Rev. 43 (2014) 5841–5866.
[20] Z. Liang, H.Y. Wang, H. Zheng, W. Zhang, R. Cao, Chem. Soc. Rev. 50 (2021) 2540–2581.
[21] J. Liu, L. Chen, H. Cui, et al., Chem. Soc. Rev. 43 (2014) 6011–6061.
[22] Y. Wang, X. Zhang, H. Lei, et al., CCS Chem. 4 (2022) 2959–2967.
[23] H. Li, H. Ye, X. Zhao, et al., Chin. Chem. Lett. 32 (2021) 2851–2855.
[24] K. Guo, X. Li, H. Lei, et al., Angew. Chem. Int. Ed. 61 (2022) e202209602.
[25] K. Guo, H. Lei, X. Li, et al., Chin. J. Catal. 42 (2021) 1439–1444.
[26] Y. Zhang, K. Ren, L. Wang, L. Wang, Z. Fan, Chin. Chem. Lett. 33 (2022) 33–60.
[27] H.Q. Xu, J. Hu, D. Wang, et al., J. Am. Chem. Soc. 137 (2015) 13440–13443.
[28] C. Xu, H. Liu, D. Li, J.H. Sub, H.L. Jiang, Chem. Sci. 9 (2018) 3152–3158.
[29] J. Liang, Y.Q. Xie, Q. Wu, et al., Inorg. Chem. 57 (2018) 2584–2593.
[30] Y.R. Wang, Q. Huang, C.T. He, et al., Nat. Commun. 9 (2018) 4466.
[31] Y. Wang, Z. Zhou, L. Zhao, et al., ACS Appl. Mater. Interfaces 13 (2021) 10925–10932.
[32] L. Yang, P. Cai, L. Zhang, et al., J. Am. Chem. Soc. 143 (2021) 12129–12137.
[33] Q. Huang, J. Liu, L. Feng, et al., Natl. Sci. Rev. 7 (2020) 53–63.
[34] H. Hu, L. Zeng, Z. Li, T. Zhu, C. Wang, Chin. J. Catal. 42 (2021) 1345–1351.
[35] Z. Liang, H. Guo, H. Lei, R. Cao, Chin. Chem. Lett. 33 (2022) 3999–4002.
[36] S. Li, J.H. Wang, L.Z. Dong, et al., Chin. Chem. Lett. 34 (2023) 107633.
[37] Y. Wang, H. Cui, Z. Wei, et al., Chem. Sci. 8 (2017) 775–780.
[38] J. Liu, Y.Z. Fan, X. Li, et al., Appl. Catal. B 231 (2018) 173–181.
[39] S. Li, H. Mei, S. Yao, et al., Chem. Sci. 10 (2019) 10577–10585.
[40] J. Liu, Y.Z. Fan, K. Zhang, L. Zhang, C.Y. Su, J. Am. Chem. Soc. 142 (2020) 14548–14556.
[41] C. Chen, Q. Mo, J. Fu, et al., ACS Catal. 12 (2022) 3604–3614.
[42] R. Makiura, O. Konovalov, Dalton Trans. 42 (2013) 15931–15936.
[43] R. Makiura, R. Usui, Y. Sakai, et al., ChemPlusChem 79 (2014) 1352–1360.
[44] R. Makiura, S. Motoyama, Y. Umemura, et al., Nat. Mater. 9 (2010) 565–571.
[45] S. Motoyama, R. Makiura, O. Sakata, H. Kitagawa, J. Am. Chem. Soc. 133 (2011) 5640–5643.
[46] C. Wang, F.F. Liu, Z. Tan, et al., Adv. Funct. Mater. 30 (2020) 1908804.
[47] M. Zhao, Y. Wang, Q. Ma, et al., Adv. Mater. 27 (2015) 7372–7378.
[48] Y. Wang, M. Zhao, J. Ping, et al., Adv. Mater. 28 (2016) 4149–4155.
[49] Q. Zuo, T. Liu, C. Chen, et al., Angew. Chem. Int. Ed. 58 (2019) 10198–10203.
[50] L. Yea, Y. Gao, S. Cao, et al., Appl. Catal. B 227 (2018) 54–60.
[51] D. Yang, S. Zuo, H. Yang, Y. Zhou, X. Wang, Angew. Chem. Int. Ed. 59 (2020) 18954–18959.
[52] W. Zhao, W. Wang, J. Peng, et al., Dalton Trans. 48 (2019) 9631–9638.
[53] T. He, B. Ni, S. Zhang, et al., Small 14 (2018) 1703929.
[54] Y. Xiao, W. Guo, H. Chen, et al., Mater. Chem. Front. 3 (2019) 1580–1585.
[55] Y. Wang, L. Feng, J. Pang, et al., Adv. Sci. 6 (2019) 1802059.
[56] Z.W. Jiang, Y.C. Zou, T.T. Zhao, et al., Angew. Chem. Int. Ed. 59 (2020) 3300–3306.
[57] Y. Zhao, J. Wang, R. Pei, J. Am. Chem. Soc. 142 (2020) 10331–10336.
[58] Y. Zhou, L. Zheng, D. Yang, et al., Small Methods 5 (2020) 2000991.
[59] J. Dong, Q. Mo, Y. Wang, et al., Chem. Eur. J. 28 (2022) e202200555.
[60] W. Yang, H. Zuo, W.Y. Lai, et al., Organometallics 34 (2015) 4051–4057.
[61] C. Chen, K.S. Chan, Organometallics 36 (2017) 3456–3464.
[62] C.W. Cheung, K.S. Chan, Organometallics 30 (2011) 4999–5009.
[63] Y.Y. Qian, K.S. Chan, Organometallics 31 (2012) 5452–5462.
[64] C.W. Cheung, K.S. Chan, Organometallics 30 (2011) 4269–4283.
[65] Y.Y. Qian, B.Z. Li, K.S. Chan, Organometallics 32 (2013) 1567–1570.
[66] S. Mori, S. Saito, Green Chem. 23 (2021) 3575–3580.
[67] K.S. Chan, C.M. Lau, Organometallics 25 (2006) 260–265.
[68] Y.Y. Qian, M.H. Lee, W. Yang, K.S. Chan, J. Organomet. Chem. 791 (2015) 82–89.
[69] L. Zhang, K.S. Chan, Organometallics 25 (2006) 4822–4829.
[70] A.F. Perez-Cadenas, F.J. Maldonado-Hodar, C. Moreno-Castilla, Carbon 41 (2003) 473–478.
[71] J.L.F. Díaz, F.L. Urías, E.M. Sandoval, Carbon 164 (2020) 324–336.
[72] A.B. Kroner, M.A. Newton, M. Tromp, et al., ChemPhysChem 14 (2013) 3606–3617.
[73] T. Nishino, M. Saruyama, Z. Li, et al., Chem. Sci. 11 (2020) 6862–6867.
[74] Y. Dwivedi, S.N. Thakur, S.B. Rai, Spectrochim. Acta Part A 71 (2009) 1952–1958.
[75] Y. Chen, M. Bouvet, T. Sizun, et al., Phys. Chem. Chem. Phys. 12 (2010) 12851–12861.
[76] Y. Chen, X. Kong, G. Lu, et al., Mater. Chem. Front. 2 (2018) 1009–1016.
[77] N.C. Maiti, S. Mazumdar, N. Periasamy, J. Phys. Chem. B 102 (1998) 1528–1538.
[78] D. Feng, Z.Y. Gu, J.R. Li, et al., Angew. Chem. Int. Ed. 51 (2012) 10307–10310.
[79] J. Qin, P. Xu, Y. Huang, et al., Chem. Commun. 57 (2021) 8468–8471.
[80] J. Rezac, P. Hobza, J. Chem. Theory Comput. 8 (2012) 141–151.
[81] Z. Fang, T. Liu, J. Liu, et al., J. Am. Chem. Soc. 142 (2020) 12515–12523.
[82] D. Lv, R. Shi, Y. Chen, et al., Ind. Eng. Chem. Res. 57 (2018) 12215 -1222.